IEEE Access
Multidisciplinary | Rapid Review | Open Access Journal

Received October 15, 2021, accepted October 26, 2021, date of publication October 27, 2021, date of current version November 8, 2021.

*Digital Object Identifier 10.1109/ACCESS.2021.3123835*

# An Investigation on the Effects of Wind Flow on Real-Time Structural Health Monitoring With Lamb Wave-Based Technique

**GUANGCHENG ZHANG[1,2], HAO JIN[1], AND YUEH-JAW LIN[2]**
[1]School of Mechanical Engineering, University of Shanghai for Science and Technology, Shanghai 200093, China
[2]College of Engineering and Engineering Technology, Northern Illinois University, DeKalb, IL 60115, USA

Corresponding author: Guangcheng Zhang (g.c.zhang@outlook.com)

**ABSTRACT** In this paper, the effects of wind flow on real-time structural health monitoring (SHM) with Lamb wave-based technique is studied with the dedicated experimental platform. Firstly, the environmental signal coming from the wind-induced vibration is observed at experimental conditions with different wind speeds by using a couple (two) of piezoelectric transducers. In order to optimize the received signal for real-time monitoring, the shunt resistor, working as the filter for the signal processing, is introduced to suppress the low-frequency noise from the wind-induced vibration. Both experimental and modeling work have been conducted to cross verify the results. Moreover, the specimen with the shunt resistor has been tested at different wind speeds condition with proper results. Furthermore, in order to verify the feasibility for practical real-time SHM, the test with only one piece of piezoelectric transducer operated as sensor and actuator simultaneously has also been conducted, and the environmental signal could be filtered as expected. The work studies the effects of wind flow on real-time SHM with Lamb wave-based technique and the signal processing method is proposed to eliminate the resultant effects, which could be applied into the real-time aircraft health monitoring.

**INDEX TERMS** Effects of wind flow, real-time SHM, Lamb wave propagation, piezoelectric transducer, aircraft skin.

## I. INTRODUCTION

In the past decades, structural health monitoring (SHM) is extensively utilized in aircraft industry [1], [2]. To prevent fatigue cracking and other subtle damage from accumulation and leading to catastrophic failure, aircrafts are needed to be monitored closely. However, considering the accuracy and feasibility of the method, there are still many problems need to be solved once applying the SHM into practical application. Consequently, the study on the reliability of the SHM in the real working environment is important and necessary [3]–[5].

The SHM process is the observation of a system utilizing dynamic response measurement with periodic sampling from a set of sensors [6]. Through this way, the damage will be detected promptly with high confidence to ensure the safe flight of the aircraft. As the main component of the aircraft, the real-time SHM of aircraft skin is of significance. In practice, a variety of techniques are widely applied to detect the damage of the aircraft skin [7], such as Acoustic Emission (AE) testing, Eddy Current Testing (ECT), Infrared Thermography (IRT). However, most of these testing methods suffer from some limitations on the aircraft applications due to their self-defects (the high cost and large size of equipment), difficult explanation on the measured signal [8]–[10], and the required working conditions [11]–[14].

In most of the off-line non-destructive test methods, the healthy aircraft may be grounded for inspection instead of being put to use. If feasible, it would be better to do condition-based monitoring, where an aircraft is continuously monitored by embedded, on-board diagnostic systems and only taken out of service when there is an actual problem. Such a prospect is still the subject of research. One of these paths of research involves permanently bonding piezoelectric wafers to the panels that make up the aircraft skin and using them as

The associate editor coordinating the review of this manuscript and approving it for publication was Gokhan Apaydin.

ultrasonic transducers in the manner described above. This would be called an embedded SHM [15], [16].

Even though, the embedded SHM has been widely studied in the aircraft skin application, the operational and environmental changes of the structure cannot be ignored during monitoring. The baseline-based signal is vulnerable to unexpected variations along with the changes of the working conditions, such as wind-induced vibration, humidity, etc. [3]–[5]. Effective compensation methods are needed to address the problems which are caused by the environmental factors.

Lamb wave have been developed to be applied into the SHM for aircrafts, which can monitor the plane in real-time and improve its reliability and security [17], [18]. The piezoelectric transducers attached to the surface of thin panels are widely used to generate Lamb waves. It is able to detect large areas and locate the damage accurately due to its low attenuation and damage sensitiveness [19]. Lamb wave was first discovered by Lamb in 1917. At the request of Sperry Product, Inc for the nondestructive evaluation of sheet metal, Firestone and Ling explored the use of these excitation in 1949 and were first to refer to the wave mode as Lamb waves in 1951. The experimental phenomenology and analytical behavior were established [20]. After decades of developing, Lamb wave have dramatic advances in charactering defects in thin plate.

In the field of fluid dynamics, there are many studies of the effects of wind flow on the aircraft wings; it is known that the wind-induced vibration will be caused during the flight of aircraft [21]. The resultant noise caused by external factors will inevitably affect the performance of the detection with ultrasonic SHM technique [22], since the identification of the testing results and the information of the fatigue and other damage will be easily masked. And there is little research on the influence of wind flow on real-time SHM for this moment. Thus, it is meaningful to study on the effects of wind flow on real-time SHM with Lamb wave-based technique and the aim is to remove the resultant noise caused by wind from the signal.

In this paper, in order to study the effects of wind flow on real-time SHM with Lamb wave-based technique, a couple (two) pieces of the piezoelectric actuator and sensor are firstly utilized to simulate the health condition of the aircraft skin in real-time, both the theoretical and experimental methods will be applied to cross verify the result. Besides that, to deal with the environmental signal that caused by the wind flow, the shunt resistor is introduced to the circuit design to work as the filter to suppress the noise of the signal caused by the wind-induced vibration. Through this way, the measured signal can be effectively processed and it will contribute to the analysis of the signal. Moreover, a single piezoelectric transducer which acts as both the actuator and sensor will be studied to simplify the structure of the test, and the possibility of the practical application for the proposed method is discussed and verified.

## II. STRUCTURE AND PRINCIPLE

To deal with the effects of wind flow on real-time SHM with Lamb wave-based technique, the experimental system was designed, and the schematic diagram of the proposed structure is shown in Figure 1. The aluminum plate was meant to be a simplified simulation of an exterior aircraft panel of a fuselage or a wing. Wind from a wind tunnel was to flow over the top of it, while the underside was to be shielded from the wind, as would be the case in a real aircraft panel. For the setup structure, the PZT transducer received Lamb waves that in a real health monitoring system would be echoes from cracks or other damage and the receiver acted as simulated damage. Considering the propagation of the Lamb wave, in this paper, the Lamb wave was firstly transmitted by the PZT transducer, then the transmitted signal and the corresponding echo reached the Lamb wave receiver in sequence. The position of the crack can be calculated directly by the location of the wave packets. The voltage signal for the piezoelectric actuators used in this experiment was delivered by an arbitrary waveform generator. The digital storage oscilloscope, controlled by a laptop, was used to receive a voltage signal from a piezoelectric sensor. The schematic experimental setup can be seen in Figure 2. The oscilloscope could capture a snapshot of the signal from a piezoelectric transducer displayed on the oscilloscope.

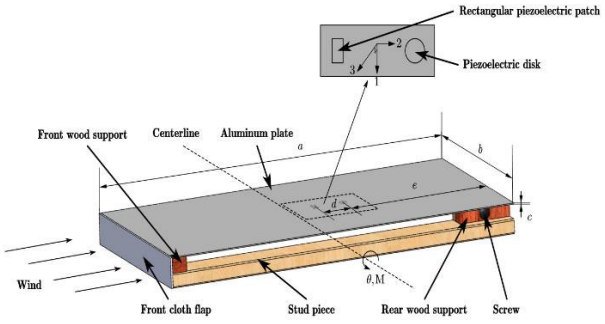


**FIGURE 1.** Schematic of the proposed structure.

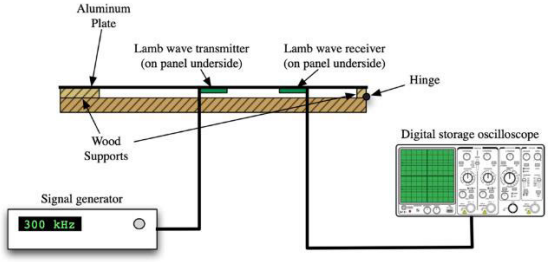


**FIGURE 2.** Schematic experimental setup.

Due to the effect of the upper and lower interface of the plate, the vibration displacement of the particle is different. Lamb wave can be divided into two types: symmetric and

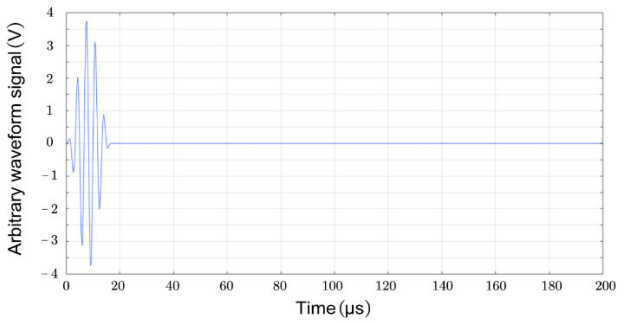


**FIGURE 3.** 9 V peak-to peak Hanning-windowed five-cycle sinusoidal wave burst with a center frequency of 300 kHz.

anti-symmetric, the dispersion equations formulated by [23], shown as:

$$\frac{\tan(qh)}{\tan(ph)} = -\frac{4k^2pq}{\left(q^2-k^2\right)^2} \text{ for symmetric Lamb wave,}$$

$$\frac{\tan(qh)}{\tan(ph)} = -\frac{\left(q^2-k^2\right)^2}{4k^2pq} \text{ for anti-symmetric Lamb wave,}$$

$$p^2 = \frac{\omega^2}{v_l^2} - k^2 \tag{1}$$

$$q^2 = \frac{\omega^2}{v_t^2} - k^2 \tag{2}$$

$$k = \frac{\omega}{v_p} \tag{3}$$

$$v_g = \frac{v_p}{1 - \frac{\omega}{v_p}\cdot\frac{dv_p}{d\omega}} \tag{4}$$

where $h$, $k$, $v_l$, $v_t$, $v_p$, $v_g$, $\omega$ are the plate thickness, wavenumber, velocities of longitudinal and transverse modes, phase velocity, group velocity and wave circular frequency, respectively.

The Lamb wave equation are converted into the relationship between phase velocity and frequency-thickness product, where the shear wave velocity $v_t$ of aluminum plate is 3110 m/s and the longitudinal wave velocity $v_l$ is 6370 m/s. In this paper, the arbitrary waveform generator was set to output a 9 V peak-to-peak Hanning-windowed five-cycle sinusoidal wave burst with a center frequency of 300 kHz. This burst was sent once every second (shown in Figure 3). In this case, the Lamb wave equation is simulated by MATLAB, the thickness of the plate was 1.6 mm, then the frequency-thickness product was 0.48; hence, the propagation speed of the Lamb wave at the frequency 300 kHz is 5006 m/s theoretically. Based on the frequency and velocity, the wave is propagating as the $S_0$ mode.

For most of the experiments in this paper, there were two piezoelectric transducers attached to the plate by epoxy adhesive (shown in Figure 1). One was a disk of PSI-5A4E material with a diameter of 12.7 mm and a thickness of 0.1905 mm, with sputtered nickel electrodes, manufactured by Piezo Systems, Inc. The other was a rectangular QuickPack QP10S transducer from Mide Technology Corporation, with piezoelectric wafer dimensions of 12.7 mm×6.35 mm×0.254 mm, and wafer material is PZT- 5A. Its capacitance was 5 nF.

According to the piezoelectric constitutive relationship, the mechanical strain tensor M and the displacement due to electrical effect in the piezoelectric patch S can be established as follows [24], [25],

$$\begin{bmatrix} \boldsymbol{M} \\ \boldsymbol{S} \end{bmatrix} = \begin{bmatrix} d & \boldsymbol{S^E} \\ \boldsymbol{\varepsilon^T} & \boldsymbol{d_t} \end{bmatrix} \begin{bmatrix} \boldsymbol{E} \\ \boldsymbol{N} \end{bmatrix} \tag{5}$$

In (5), M = mechanical strain tensor, N= mechanical stress tensor, d stands for the inverse piezoelectric coefficient, $S^E$ = elasticity matrix, and $\varepsilon^T$ represents the dielectric constant of the underlying piezoelectric material. In addition, other parameters such as $d_t$ = piezoelectric coefficient tensor, should be considered the same as $d$.

In our consideration in this work, the upper and lower sides of the PZT patch were chosen to be the electrode terminals. Along the same line, the direction of poling was aligned with the third axis.

The strain of the plate changed along with the propagation of the Lamb wave, which will be captured by the piezoelectric patch attached on it.

## III. ANALYTICAL MODELING

In this paper, a finite element software (COMSOL) is used to simulate the detection of the plate with Lamb wave. Both the propagation of the Lamb wave simulation and the natural frequencies of the plate are studied in the section. In order to allow for a time-efficient computation, a 2-dimensional approach is employed. Strictly speaking the proposed SHM system is 3-dimensional, but it is believed that a 2D approach is sufficiently accurate and permits us to use Computational Fluid Dynamic (CFD) calculations as predictive tool once considering air flow in the following discussion.

For the simulation on the propagation of the Lamb wave, the Finite Element Method (FEM) of the structure is shown in Figure 4, mapped which can generate structured quadrilateral mesh is used to mesh the domain of two piezoelectric transducers and the maximum element size is set as 0.1mm. The triangular elements are used to mesh the domain of aluminum plate and element size is set as extremely fine (the average element quality is 0.8804). The excitation signal is set as Hanning-windowed five-cycle sinusoidal wave burst with a center frequency of 300 kHz. The output times of study setting is set as range of 0 to 70∗T, times step is T/20, and the tolerance is set as physics controlled. In this simulation test, the global method of absolute tolerance is set as Scaled, tolerance method is chosen as Factor and the factor is 0.1. In time stepping, generalized alpha is chosen as the method, steps taken by solver is set as Manual and time step is 1/(10∗f), amplification for high frequency is 0.5. The result is shown in Figure 5.

The first peak of the graph shows the Lamb wave firstly reached the piezoelectric sensor. It can be known the propagation time that the wave to travel from piezoelectric actuator

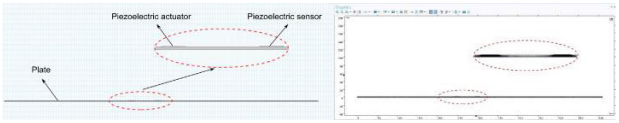


**FIGURE 4.** FEM of the plate.

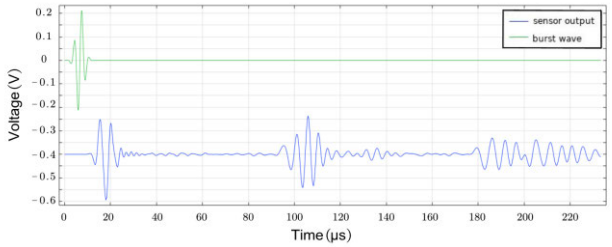


**FIGURE 5.** Relationship between output voltage and time.

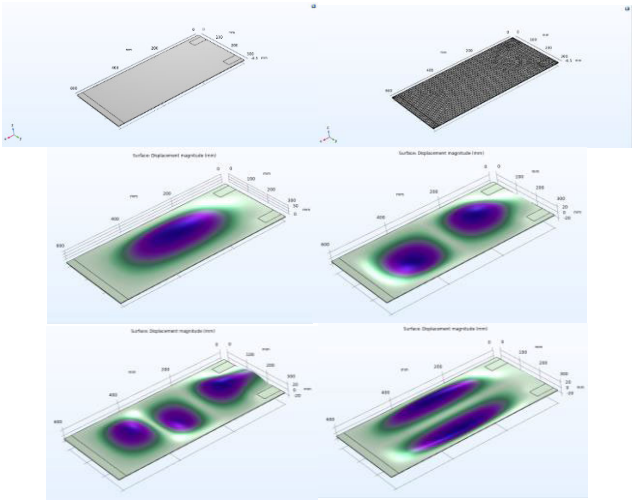

**FIGURE 6.** FEM model of the plate and vibration modes.

to piezoelectric sensor and the distance between piezoelectric actuator and piezoelectric sensor has been told. Then the second peak generates once the wave echoes back from the rear edge. The third one indicated the reflect wave from front edge. Based on the simulation, the propagation speed of the Lamb wave is calculated at approximately 5 km/s which is corresponding to the earlier theoretical study which means that the FEM model is reliable.

The natural frequencies of the plate were estimated by the simulation on the vibration mode, the effects of the wood supports were modeled by boundary conditions imposed on the plate. The FEM model of the structure is shown is shown in Figure 6. It demonstrates that the first forth natural frequencies of the plate are approximately 80.652, 141.84, 228.17, and 242.16 Hz.

In order to analyze the signal response of the piezoelectric transducer at different wind speeds, an FEM of the plate considering the couples of the fluid dynamic, mechanics, piezoelectric effect are established (shown in Figure 7). In the

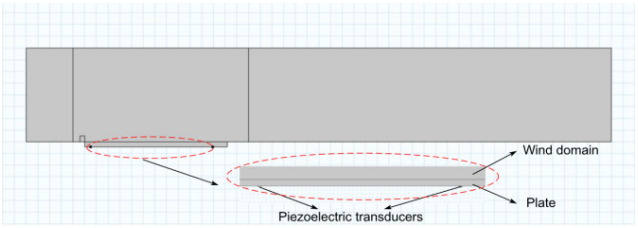


**FIGURE 7.** FEM of the plate and the fluid field.

modeling, the size of two piezoelectric transducers is reduced to 1 mm to avoid the effect of the size of the piezoelectric transducers.

Draw the wind domain above the aluminum plate, and set the left side of the domain as the inlet, the velocity is set as 17[m/s]∗(Y+0.2[m])∗(0.2[m]-Y)/(0.4[m]/2)^2, set the right side of the domain as the outlet, its Boundary Condition is set as Pressure, Pressure Condition is set as Static and check the Suppress backflow option.

Mapped is used to mesh the domain of two piezoelectric transducers and the maximum element size is set as 0.1mm. The triangular elements are used to mesh the remaining domain and element size is set as extremely fine (the average element quality is 0.7752), as shown in Figure 8. The output signal of the piezoelectric transducer is shown on the Figure 9, when the wind speed is 17 m/s. And contour of the flow can be seen in Figure 10. It is believed that the vibration of the plate will be induced by the fluid dynamics, such as vortex shedding and the impact of the vortex.

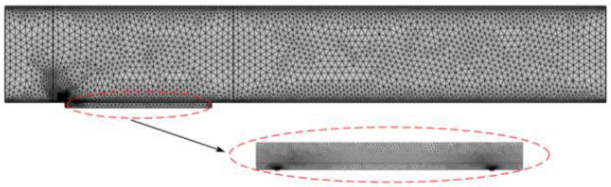

**FIGURE 8.** Meshing.

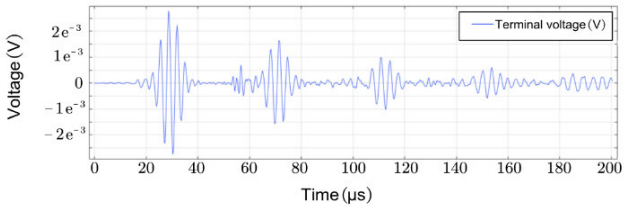


**FIGURE 9.** The output signal of the piezoelectric transducer.

## IV. EXPERIMENTAL SETUP

As shown in Figure 11, the structure of the specimen is fixed in the wind tunnel and the top of the specimen was an aluminum plate which is 609.6 mm long, 304.8 mm

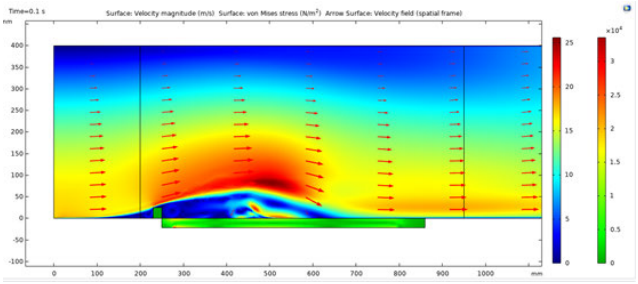

**FIGURE 10.** Contour of the flow.

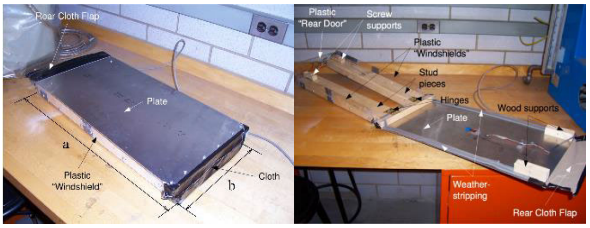


**FIGURE 11.** The structure of the specimen.

**TABLE 1.** The geometric and material parameters of the piezoelectric material and the experimental system.

| Parameters | Values |
|---|---|
| a-the length of plate (mm) | 609.6 |
| b (mm) | 304.8 |
| c (mm) | 1.6 |
| d (mm) | 50.8 |
| e (mm) | 241.3 |
| The diameter of piezoelectric disk (mm) | 12.7 |
| The thickness of piezoelectric disk (mm) | 0.1905 |
| The length of rectangular piezoelectric patch (mm) | 12.7 |
| The width of rectangular piezoelectric patch (mm) | 6.35 |
| The thickness of rectangular piezoelectric (mm) | 0.254 |
| The maximum wind speed of the wind tunnel (m/s) | 31.3 |
| The height of wood supports (mm) | 25.4 |
| The length of wooden stud (mm) | 88.9 |
| The width of wooden stud (mm) | 38.1 |
| The length of the front wood support (mm) | 304.8 |
| The width of the front wood support (mm) | 25.4 |
| The length of the rear wood support (mm) | 88.9 |
| The width of the rear wood support (mm) | 25.4 |
| The distance between the side edges of the rear supports and the side edges of the plate (mm) | 19.05 |
| The maximum sampling rate for the DAQ board (kHz) | 500 |
| The input resistance of the DAQ board (GΩ) | 100 |
| The capacitance of rectangular piezoelectric (nF) | 5 |
| The resistance of the waveform generator (Ω) | 50 |
| The input resistance of the HP 54602B digital storage oscilloscope(MΩ) | 1 |

wide and 1.6 mm thick. Attached to the stud pieces were ''windshields'' made of scrap plastic, to help keep wind from reaching the underside of the aluminum plate from the sides. Foam weatherstripping was placed near the edges of the plate to seal the space between the plastic shields and the plate. The detailed geometric and material parameters are shown in table 1.

The wind tunnel used in the experiments was relatively small. The maximum wind speed was approximately 31.3 m/s. Its cross-section was about 77.4 $cm^2$, and it could only accommodate a specimen about 914.4 mm long at most. There were circular holes in the floor of this space in the wind tunnel, and bolts, screws, etc., could be put through these holes in order to mount specimens. The manometer displayed pressure changes in inches of water. Figure 12 shows the specimen in the wind tunnel and the placement of the manometer, as well as the testing equipment used in this experiment.

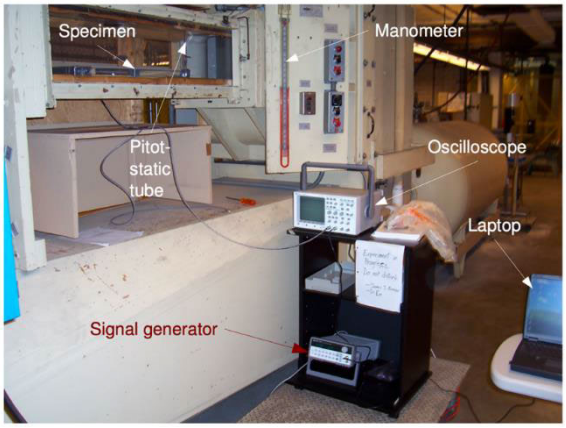


**FIGURE 12.** Setup of the experiment.

The voltage signal for the piezoelectric actuators used in this experiment was delivered by an HP 33120A arbitrary waveform generator. The waveform generator has a fixed output resistance of 50 Ω. HP 54602B digital storage oscilloscope, controlled by a laptop, was used to receive a voltage signal from a piezoelectric sensor.

## V. DISCUSSION OF EXPERIMENTAL RESULTS AND CHARACTERISTICS

During the experiment, the specimen was bolted into the wind tunnel. Channel 1 of the digital oscilloscope was connected to the QuickPack transducer, which served as a sensor. The arbitrary waveform generator was set to output a 9 V peak-to-peak Hanning-windowed five-cycle sinusoidal wave burst with a center frequency of 300 kHz. This burst was sent once every second. This was connected both to channel 2 of the oscilloscope, so that the signal could be viewed, if need be, and to the piezoelectric disk from Piezo Systems, Inc., which served as an actuator. The oscilloscope was set to trigger on an external signal input to channel 3, provided by a synchronization signal from the arbitrary waveform generator.

For each wind speed represented by the wind tunnel, the response of the sensor output at the speed, 17 m/s, can be seen in Figure 13. The signal show the Lamb wave pulse received by the sensor, which acts as a crack, from the transmitter, as well as pulses reflected from the edges of the specimen. As shown in Figure 13, there is an increasing trend of the received signal on the time length of the experiment.

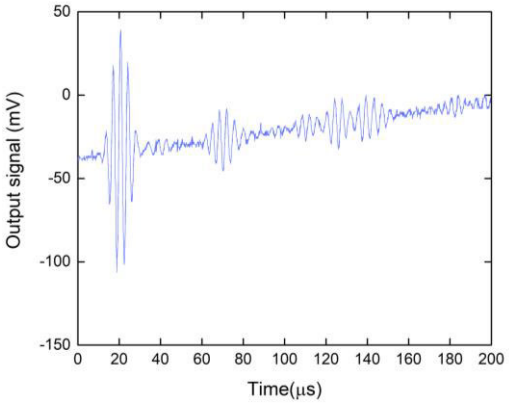


**FIGURE 13.** Sensor output at 17m/s.

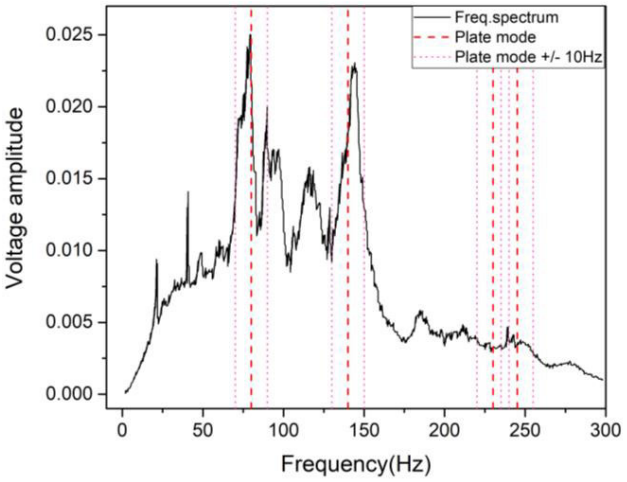


**FIGURE 14.** Amplitude spectrum at 17 m/s wind speed, with lines indicating natural frequencies.

Compared with the results of simulation without wind flow, even the propagation of the wave packets of these two are consistent with each other, it will affect the accuracy of damage detection. The reasons may come from the superimposition of the rising edge of the low-frequency environmental signal generated by the wind-induced vibration and the Lamb wave packets.

Fast Fourier transform (FFT) is also conducted in the paper to explain the results from the experiment. For the given wind speed at 17 m/s, the set of 2,097,152 samples per signal capture was split into 128 subsets of 16,384 samples. A Hanning-windowed was applied to each of these subsets, and then a 16,384-point FFT was done on each of them. Then the resulting amplitude spectra, all 128 of them, were averaged together. Figure 14 show the part of low-frequency spectra, and also indicate the natural frequencies as determined by COMSOL, which is shown in Figure 6, with lines also indicating the frequencies $\pm 10$ Hz of those found natural frequencies by COMSOL. Overall, the peaks of processed experimental data are corresponding to the natural frequencies of the plate from the modal analysis, and it is easily understood that the peaks are caused by resonant vibration of the plate.

It is easily understood that the accuracy of the damage detection mainly relies on the quality of the received signal from the piezoelectric transducer. In order to optimize the received signal, according to the property of the piezoelectric transducer, it is believed that the low-frequency noise from the wind-induced vibration could be suppressed by introducing the shunt resistor as the filter for the signal processing. From (5), $D$ and $E$ are the electric displacement and electric field, respectively, as $3 \times 1$ column vectors. $D_i$ and $E_i$ are the elements of their respective vectors in the $x_1$, $x_2$, and $x_3$ directions shown in Figure 1. S and T are the strain and stress expressed a $6 \times 1$ column vectors in Voigt notation. $\epsilon$ is the $3 \times 3$ diagonal matrix of dielectric constants, evaluated at constant stress. $s$ is the $6 \times 6$ elastic compliance matrix. A superscripted T indicates the transpose of a matrix. Hagood and von Flotow defined the column vector V such that for a rectangular piezoelectric element such as the one in Figure 14, each element $V_i$ is the potential difference between the surfaces normal to the $x_i$ direction, and they defined the column vector I such that for the same rectangular element, each element $I_i$ is the current that may flow between the surfaces normal to the $x_i$ direction.

$$V_i = \int_0^{L_i} E \cdot dx_i \tag{6}$$

$$I_i = \int_{A_i} D \cdot dA_i \tag{7}$$

where $L_i$ is the dimension of the piezoelectric element along the $x_i$ direction, and $A_i$ is the cross-sectional area normal to the $x_i$ direction. It should be noted that V and I are not true vectors in the way that D and E are. In the Laplace domain,

$$V(s) = LE(s) \tag{8}$$

$$I(s) = sAD(s) \tag{9}$$

where

$$L = \begin{bmatrix} L_1 & 0 & 0 \\ 0 & L_2 & 0 \\ 0 & 0 & L_3 \end{bmatrix} \quad A = \begin{bmatrix} A_1 & 0 & 0 \\ 0 & A_2 & 0 \\ 0 & 0 & A_3 \end{bmatrix} \tag{10}$$

Substituting (18) and (19) into (20) yields

$$\begin{bmatrix} I \\ S \end{bmatrix} = \begin{bmatrix} sA\epsilon L^{-1} & sAd \\ d^T L^{-1} & s \end{bmatrix} \begin{bmatrix} V \\ T \end{bmatrix} \tag{11}$$

For a thin piezoelectric wafer, $V_1 \approx V_2 \approx 0$, so letting $I_3 = I_{piezo}$ and $V_3 = \mathrm{V}$,

$$I_{piezo} = \frac{sA_3\epsilon_3}{L_3} V + sA_3 \sum_{i=1}^{6} d_{3i} T_i \tag{12}$$

$A_3\epsilon_3/L_3$ is the capacitance of the element, or C, so

$$I_{piezo} = sCV + sA_3 \sum_{i=1}^{6} d_{3i} T_i \tag{13}$$

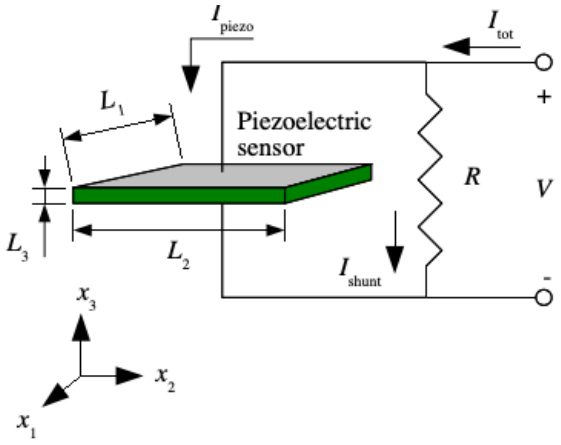


**FIGURE 15.** Shunt resistor across piezoelectric sensor.

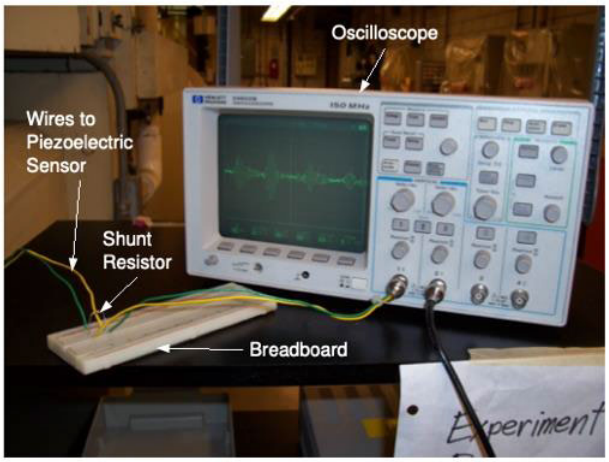


**FIGURE 16.** Photograph of shunt resistor.

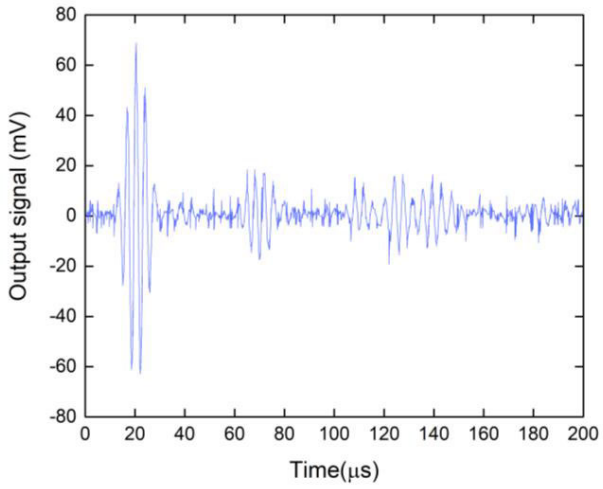


**FIGURE 17.** Sensor outputs at the speed, 17m/s, with 1 kΩ shunt resistor in place.

For the shunt shown in Figure 15, $I_{shunt}$ is simply $V/R$. The total current through the shunted piezoelectric element, then, is

$$I_{tot} = I_{piezo} + I_{shunt} = \left(sC + \frac{1}{R}\right) V + sA_3 \sum_{i=1}^{6} d_{3i} T_i \quad (14)$$

Let

$$Y_D = sC \quad (15)$$

$$Y_{EL} = sC + \frac{1}{R} \quad (16)$$

so that $I_{piezo}$ and $I_{tot}$ can expressed as

$$I_{piezo} = Y_D V + sA_3 \sum_{i=1}^{6} d_{3i} T_i \quad (17)$$

$$I_{tot} = Y_{EL} V + sA_3 \sum_{i=1}^{6} d_{3i} T_i \quad (18)$$

When there is no stress in the piezoelectric element, $Y_D$ is the admittance of the unshunted element, and $Y_{EL}$ is the admittance of the shunted element. The aforementioned $Z_D$ and $Z_{EL}$ are simply $1/Y_D$ and $1/Y_{EL}$. This leads directly to equation

$$\frac{Z_{EL}}{Z_D} = \frac{sRC}{1 + sRC} \quad (19)$$

As noted above, a simple shunt resistor across a piezoelectric sensor can filter out lower frequencies. Since the use of a shunt resistor would be simple and relatively inexpensive, it was worth investigating to see if it would be a viable filter. The corner frequency $f_c$ should be about 1 of the frequencies of interest. For the shunt resistance R = 1 kΩ, and the sensor capacitance C = 5 nF this corner frequency is

$$f_c = \frac{1}{2\pi RC} = \frac{1}{2\pi \left(1 \times 10^3 \Omega\right) \left(5 \times 10^{-9} F\right)} \approx 32 kHz \quad (20)$$

which is barely acceptable, since the center frequency of the Lamb wave pulse received by the sensor is about 300 kHz. The shunt resistance R = 1 kΩ, then, is an upper limit on the shunt resistor that would serve as a viable filter. Thus, a 1000 ± 5% Ω shunt resistor was placed in parallel to the piezoelectric sensor to test its effectiveness, as shown in Figure 16. The results of the test at the wind speed 17 m/s are shown in Figure 17.

In order to verify the feasibility of the designed filter at different working conditions, the specimen with the shunt resistor has been tested at three different wind speeds condition in the experiment. As shown in Figure 18, the propagation of wave packets with proper performance under the wind speed of 10 m/s, 17 m/s and 31 m/s, benefitting from the shunt resistor. However, the noise of the received signal is relatively more obvious at higher wind speed and it may come from the increasing strength of wind-induced vibration.

In the practical application, it is valuable if the number of the piezoelectric transducers could be decreased, not only considering the cost of the system, but also the weight of

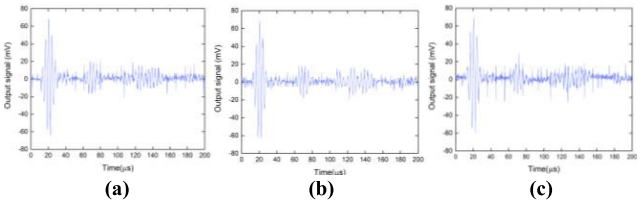


**FIGURE 18.** Sensor output at (a) 10m/s, (b) 17m/s, (c) 31m/s with shunt resistor.

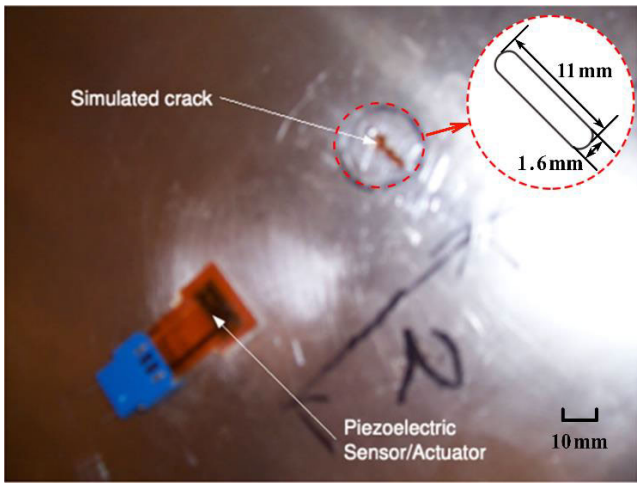


**FIGURE 19.** Photograph of simulated crack in plate.

the detecting system will be a burden to the aircraft. Consequently, the experiment with only one piezoelectric patch is conducted, the piezoelectric disk from Piezo Systems, Inc. was removed from the plate. The single piezoelectric transducer acts as both the actuator and sensor, and the source of Lamb wave and the receiving probe are at the same location. There was a roughly simulated crack made by drilling 1.6 mm holes next to each other and removing the material bridging them with an awl (a rectangular crack about 11 mm long and 1.6 mm wide). The simulated crack is shown in Figure 19.

The QuickPack transducer then was connected to both the arbitrary waveform generator and the oscilloscope to serve as both sensor and actuator. Again, the arbitrary waveform generator was set to output a 9 V peak-to-peak Hanning-windowed five-cycle sinusoidal wave burst with a center frequency of 300 kHz, and this burst was sent once every second. Between these bursts, the transducer would receive echoes reflected from the simulated crack and from the edges of the specimen. For the wind speed at 17 m/s, the signal output was captured (shown in Figure 20). Since the piezoelectric transducer operated as sensor and actuator simultaneously, both the initial pulse from the waveform generator and the resulting echoes were displayed on the oscilloscope. Through introducing the shunt resistor to the circuit design as a filter, the resultant noise of signal caused by the wind-induced vibration is suppressed. Thus, the accuracy of damage detection could be improved.

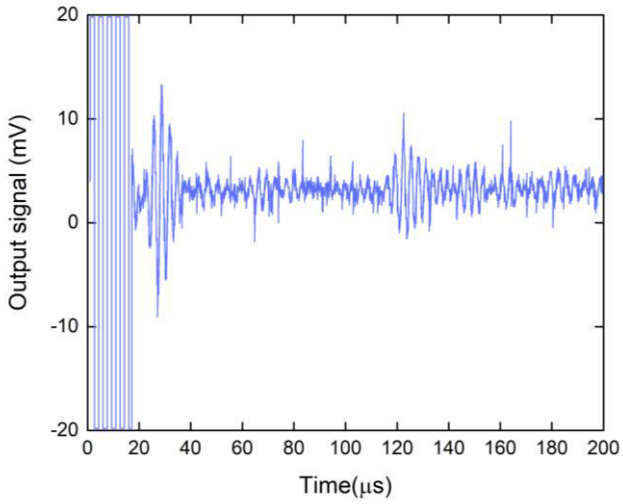


**FIGURE 20.** Sensor/actuator output at 17m/s wind speed.

## VI. SUMMARY

In this paper, an investigation on the effects of wind flow on real-time SHM with Lamb wave-based technique has been conducted. The dedicated experimental system was setup, and the specimen made by aluminum plate was designed to simulate the exterior aircraft panel of a fuselage or a wing in the wind tunnel.

Firstly, a couple (two) of piezoelectric transducers were utilized to transmit and receive the Lamb wave to detect the damage; compared with the results without wind flow, the low-frequency environmental signal coming from the wind-induced vibration was observed at experimental conditions with different wind speeds. Furthermore, the shunt resistor as the filter for the signal processing was introduced to suppress the low-frequency noise from the wind-induced vibration. Besides that, the FEM model has been conducted to cross verify the results. Benefiting from the shunt resistor, the propagation of wave packets in the experiment owes proper performance under different wind speed. Moreover, in order to verify the feasibility for practical real-time SHM, the test with only one piece of piezoelectric transducer operated as sensor and actuator simultaneously has also been conducted, and the environmental signal could be filtered as expected. Based on the study, the resultant effects from the wind-induced vibration caused by the wind flow on real-time SHM with Lamb wave-based technique could be eliminated; meanwhile, the reliability of SHM in the real working environment has been improved, which has great help in the application of the real-time aircraft health monitoring.

In future studies, we will focus on the analysis of the filtered signal to apply the study into real aircraft wings, fuselage and related applications.

## REFERENCES

[1] L. Qiu, S. Yuan, and C. Boller, "An adaptive guided wave-Gaussian mixture model for damage monitoring under time-varying conditions: Validation in a full-scale aircraft fatigue test," *Struct. Health Monitor.*, vol. 16, no. 5, pp. 501–517, Sep. 2017.

[2] M. Mitra and S. Gopalakrishnan, "Guided wave based structural health monitoring: A review," *Smart Mater. Struct.*, vol. 25, no. 5, May 2016, Art. no. 053001.
[3] V. Giurgiutiu and A. Cuc, "Embedded non-destructive evaluation for structural health monitoring, damage detection, and failure prevention," *Shock Vib. Dig.*, vol. 37, no. 2, p. 83, 2005.
[4] S. Roy, P. Ladpli, and F.-K. Chang, "Load monitoring and compensation strategies for guided-waves based structural health monitoring using piezoelectric transducers," *J. Sound Vib.*, vol. 351, pp. 206–220, Sep. 2015.
[5] Y. Ren, L. Qiu, S. Yuan, and F. Fang, "Multi-damage imaging of composite structures under environmental and operational conditions using guided wave and Gaussian mixture model," *Smart Mater. Struct.*, vol. 28, no. 11, Nov. 2019, Art. no. 115017.
[6] G. C. Kahandawa, J. Epaarachchi, H. Wang, and K. T. Lau, "Use of FBG sensors for SHM in aerospace structures," *Photon. Sensors*, vol. 2, no. 3, pp. 203–214, 2012.
[7] X. Qing, W. Li, Y. Wang, and H. Sun, "Piezoelectric transducer-based structural health monitoring for aircraft applications," *Sensors*, vol. 19, no. 3, p. 545, Jan. 2019.
[8] J. Huang, *Non-Destructive Evaluation (NDE) of Composites: Acoustic Emission (AE), In Non-Destructive Evaluation (NDE) of Polymer Matrix Composites*. Amsterdam, The Netherlands: Elsevier, 2013, pp. 12–32.
[9] J. García-Martín, J. Gómez-Gil, and E. Vázquez-Sánchez, "Non-destructive techniques based on eddy current testing," *Sensors*, vol. 11, no. 3, pp. 2525–2565, Feb. 2011.
[10] J. Cheng, J. Qiu, H. Ji, E. Wang, T. Takagi, and T. Uchimoto, "Application of low frequency ECT method in noncontact detection and visualization of CFRP material," *Compos. B, Eng.*, vol. 110, pp. 141–152, Feb. 2017.
[11] C. Maierhofer, "Characterizing damage in CFRP structures using flash thermography in reflection and transmission configurations," *Compos. B, Eng.*, vol. 57, pp. 35–46, Jun. 2014.
[12] R. Usamentiaga, P. Venegas, J. Guerediaga, L. Vega, J. Molleda, and F. G. Bulnes, "Infrared thermography for temperature measurement and non-destructive testing," *Sensors*, vol. 14, no. 7, pp. 12305–12348, 2014.
[13] C. Meola S. Boccardi, G. M. Carlomagno, N. D. Boffa, and R. Russo, "Impact damaging of composites through online monitoring and non-destructive evaluation with infrared thermography," *NDT E Int.*, vol. 85, pp. 34–42, Jan. 2017.
[14] F. Ciampa, P. Mahmoodi, F. Pinto, and M. Meo, "Recent advances in active infrared thermography for non-destructive testing of aerospace components," *Sensors*, vol. 18, no. 2, p. 609, Feb. 2018.
[15] H. Rocha, C. Semprimoschnig, and J. P. Nunes, "Sensors for process and structural health monitoring of aerospace composites: A review," *Eng. Struct.*, vol. 237, Jun. 2021, Art. no. 112231.
[16] H.-Y. Tang, C. Winkelmann, W. Lestari, and V. La Saponara, "Composite structural health monitoring through use of embedded PZT sensors," *J. Intell. Mater. Syst. Struct.*, vol. 22, no. 8, pp. 739–755, May 2011.
[17] Y. Wang, L. Qiu, Y. Luo, R. Ding, and F. Jiang, "A piezoelectric sensor network with shared signal transmission wires for structural health monitoring of aircraft smart skin," *Mech. Syst. Signal Process.*, vol. 141, Jul. 2020, Art. no. 106730.
[18] Z. Hanfei, C. Shuhao, M. Shiwei, L. Yu, X. Hanyu, X. Qingwei, L. Yanyan, and Z. Haiyan, "Multi-sensor network for industrial metal plate structure monitoring via time reversal ultrasonic guided wave," *Measurement*, vol. 152, Feb. 2020, Art. no. 107345.
[19] P. Cawley and D. Alleyne, "The use of Lamb waves for the long range inspection of large structures," *Ultrasonics*, vol. 34, nos. 2–5, pp. 287–290, Jun. 1996.
[20] Z. Su, L. Ye, and Y. Lu, "Guided Lamb waves for identification of damage in composite structures: A review," *J. Sound Vib.*, vol. 295, nos. 3–5, pp. 753–780, Aug. 2006.
[21] D. Lee, J. Im, H. Lee, Y. Jung, J. Jeong, J.-H. Shin, S. Lee, J. H. Park, and J. Ahn, "Modeling and simulation of aircraft motion for performance assessment of airborne AESA radar considering wind and vibration," *J. Korean Soc. Aeronaut. Space Sci.*, vol. 48, no. 11, pp. 903–910, Nov. 2020.
[22] H. Wang, B. Zhang, G. Y. Tian, D. Zhou, P. Wang, and Y. Li, "The research on the flaw classification and identification of the PEC NDT technology," *Int. J. Appl. Electromagn. Mech.*, vol. 33, nos. 3–4, pp. 1343–1349, Oct. 2010.
[23] J. Achenbach, *Wave Propagation in Elastic Solids*. Amsterdam, The Netherlands: Elsevier, 2012.
[24] T. R. Meeker, "Publication and proposed revision of ANSI/IEEE Standard 176-1987 'ANSI/IEEE Standard on piezoelectricity,'" *IEEE Trans. Ultrason., Ferroelectr., Freq. Control*, vol. 43, no. 5, p. 717, Sep. 1996.
[25] F. Qian, W. Zhou, S. Kaluvan, H. Zhang, and L. Zuo, "Theoretical modeling and experimental validation of a torsional piezoelectric vibration energy harvesting system," *Smart Mater. Struct.*, vol. 27, no. 4, Apr. 2018, Art. no. 045018.

**GUANGCHENG ZHANG** received the bachelor's and master's degrees from the Nanjing University of Aeronautics and Astronautics and the Ph.D. degree from the University of Nottingham. His research interests include vibration control, energy harvesting, and smart hydraulic technology.

**HAO JIN** received the bachelor's degree from Wenzhou University. He is currently pursuing the M.S. degree with the University of Shanghai for Science and Technology. His main research interest includes piezoelectric material.

**YUEH-JAW (YJ) LIN** received the Ph.D. degree from the University of Illinois at Chicago. He is currently a Professor of mechanical engineering and the Director of mechatronics programming with Northern Illinois University. His main research interests include mechatronics engineering, applied robotics in design and automation, aircraft deicing and health monitoring, and renewable energy and energy harvesting.